Damped soft phonons and diffuse scattering in $(Bi_{1/2}Na_{1/2})TiO_3$

M. Matsuura,[1] H. Iida,[2] K. Hirota,[3] K. Ohwada,[4] Y. Noguchi,[5] and M. Miyayama[5]
[1]*Institute for Materials Research, Tohoku University, Sendai 980-8577, Japan*
[2]*Institute for Solid State Physics, The University of Tokyo, Kashiwa 277-8581, Japan*
[3]*Department of Earth and Space Science, Graduate School of Science, Osaka University, Toyonaka, 560-0043, Japan*
[4]*Synchrotron Radiation Research Center (SPring-8), Quantum Beam Science Directorate, Japan Atomic Energy Agency, Sayo, Hyogo 679-5148, Japan*
[5]*Research Center for Advanced Science and Technology, The University of Tokyo, 4-6-1 Komaba, Meguro-Ku, Tokyo 153-8904, Japan*
(Received 6 October 2012; revised manuscript received 17 January 2013; published 22 February 2013)

Neutron-scattering studies of $(Bi_{1/2}Na_{1/2})TiO_3$ (BNT) have been performed to elucidate the microscopic mechanism of the broad maximum in the temperature dependence of the dielectric constant at $T_m \sim 600$ K and the reduction in the piezoelectric properties above the depolarization temperature, $460 \sim 480$ K. We observed diffuse scattering near the Γ point below 700 K, which competes with the superlattice peak at the *M* point of the tetragonal phase but coexists with the superlattice peak at the *R* point of the rhombohedral phase. The diffuse scattering shows an anisotropic *Q* shape extending along the ⟨100⟩ direction transverse to the scattering vector *Q*, which is explained by atomic shifts bridging the tetragonal and rhombohedral structures. We propose that the broad maximum in the dielectric constant is associated with a diffusive first-order transition between the competing tetragonal and rhombohedral phases. In addition, we found that the diffuse scattering is reduced for single crystals grown under high oxygen pressure, which suggests an analogy with the central peak in hydrogen-reduced $SrTiO_3$. Inelastic neutron scattering near the Γ point reveals a heavily overdamped soft mode similar to those reported in lead-based relaxors, the "waterfall" feature. Moreover, a damped soft transverse acoustic mode is observed for the ⟨100⟩ direction as the anisotropic diffuse scattering, indicating phase instabilities with the same origin as that of the diffuse scattering. The recovery of the soft mode is observed near the depolarization temperature, which coincides with the disappearance of the superlattice peak at the *M* point. These results indicate that the depolarization and the waterfall feature originate in the dynamic nature of ferroelectric clusters in the coexisting tetragonal/rhombohedral phase.

DOI: 10.1103/PhysRevB.87.064109 PACS number(s): 77.80.−e, 61.05.F−, 63.20.D−

I. INTRODUCTION

Bismuth sodium titanate $(Bi_{1/2}Na_{1/2})TiO_3$ (BNT) is a complex ABO_3 perovskite in which the A site is randomly occupied by one of two valence cations, Na^+ and Bi^{3+}. Since the discovery of BNT by Smolenskii *et al.*,[1] its structural and ferroelectric properties have been investigated, with attention to its peculiar phase transition sequence and complex ferroelectric properties.[2] Recently, BNT and BNT-based compounds have gained considerable attention as lead-free ferroelectric or piezoelectric materials due to their relatively large spontaneous polarization and high Curie temperature (T_C).[3–5] The structural phase transition from the cubic to the tetragonal phase occurs first at 813 K. The tetragonal phase was thought to be antiferroelectric because of a pinched dielectric hysteresis loop in a solid solution of BNT and $SrTiO_3$.[6] However, a recent neutron diffraction study revealed that the tetragonal phase is ferrielectric with antiparallel atomic shifts between Bi/Na and Ti cations along the fourfold axis [001].[7] The rhombohedral phase arises at 700 K on cooling and coexists with the tetragonal phase in a wide temperature range of $200 \sim 300$ K.[8] The rhombohedral phase is ferroelectric with parallel cation shifts along the polar ⟨111⟩ axes.[7] Interestingly, the structures of the tetragonal and rhombohedral phases include tilts of the TiO_6 octahedra, an in-phase tilt about the fourfold pseudocubic axis for the tetragonal phase, and an antiphase tilt about the threefold pseudocubic axes for the rhombohedral phase, which give rise to superlattice peak at the *M* and *R* points, respectively.[8] Thus, the ferroelectric properties in the pure tetragonal phase and pure rhombohedral phase are now understood. However, the intermediate phase at which the rhombohedral and tetragonal phases coexist is not fully understood. For example, a broad maximum in the temperature dependence of the dielectric constant occurs at ∼600 K (T_m), whereas no phase transition has been observed near T_m.

Another unsolved problem in BNT is the dramatic reduction in the piezoelectric properties in the rhombohedral phase above a depolarization temperature of $460 \sim 480$ K,[9,10] which is more than 200 K lower than the onset temperature of the rhombohedral phase. It is worth mentioning that a broad maximum in the dielectric constant and depolarization without a structural phase transition have been observed in lead-based relaxors.[11,12] In these materials, nanometer-scale regions having local, randomly oriented, ferroelectric polarizations, so-called polar nanoregions (PNRs), are believed to be responsible for these peculiar features. A characteristic diffuse scattering associated with PNRs[13] and overdamping of the soft transverse optical (TO) mode[14–16] have been reported in classical relaxors with B-site disorder such as $Pb(Mg_{1/3}Nb_{2/3})TiO_3$-(PMN-) based and $Pb(Zn_{1/3}Nb_{2/3})TiO_3$- (PZN-) based compounds, although the microscopic mechanism of the diffuse scattering is still under debate.[17–21] In BNT, diffuse scattering and the soft mode near the superlattice peaks at the *M* and *R* points for the successive phase transitions have been intensively investigated.[8,22–25] Although diffuse scattering near the Γ point has been reported from neutron scattering[24] and

x-ray diffraction,[26] the detailed temperature and Q dependencies of the diffuse scattering and soft mode have not been studied yet.

In this study, we performed inelastic and elastic neutron scattering on single crystals of BNT near the Γ point to elucidate the microscopic mechanism of the broad maximum in the dielectric constant and the depolarization in BNT. We have concentrated on the diffuse scattering and phonon spectrum near the Γ point and measured q profiles and temperature dependence. This paper is organized as follows. The experimental details are described in Sec. II. The observed diffuse scattering and phonons are reported in Secs. III and IV, respectively. The origin of the broad maximum in the temperature dependence of the dielectric constant and phonon anomalies are discussed in Sec. V. A summary and conclusions are given in Sec. VI.

II. EXPERIMENTAL DETAILS

Yellowish transparent single crystals of BNT with typical dimensions of $5 \times 5 \times 5$ mm^3 were grown using a flux method under an oxygen pressure of 1 atm. The parts of the crystals used in Fig. 5 were grown under a high-oxygen-pressure atmosphere[10,27] and show lower leakage current and better polarization switching. Before the electrical measurements and neutron-scattering experiment, the crystals were annealed at 950 °C for 10 h in air to reduce the oxygen vacancies and release the strain induced during crystal growth. For the dielectric response measurements, the annealed crystals grown under high-oxygen-pressure atmosphere with a (100) face were cut into 0.1- to 0.2-mm-thick plates, and gold electrodes were sputtered onto the (100) surfaces.

Neutron-scattering studies were performed on the annealed single crystals using the University of Tokyo's triple-axis spectrometers "PONTA" and "HQR" installed at the JRR-3 reactor at the Japan Atomic Energy Agency. The horizontal collimation sequences were 40′-80′-sample-40′-80′ and Guide-40′-sample-60′-60′ for PONTA and HQR, respectively. The final neutron energies were fixed using a pyrolytic graphite (PG) analyzer to 14.7 and 30.5 meV for measurements using PONTA and to 14.7 meV for the diffuse scattering measurement using HQR. A PG filter was placed in front of the analyzer to diminish the scattering of higher-order neutrons. For the diffuse scattering study with PONTA, an additional PG filter was used in front of the sample to eliminate higher-order neutrons.

For phonon measurements, we mounted the single crystal to access the $(hk0)$ scattering plane in the pseudocubic notation. To study the distribution of the diffuse scattering in three-dimensional Q space, two scattering planes, $(hk0)$ and (hkk), were used. Reciprocal lattice units (rlu) are used where 1 rlu $= 2\pi/a$, and $a = 3.887$ Å is the room temperature lattice parameter in the pseudocubic notation.

The phonon intensities of the same scans shown in Fig. 6 and Fig. 9 differ by a factor of ∼2 due to different final neutron energies (E_f). For E_f of 30.5 meV, contamination by higher-order neutrons is less than 10%, whereas the ratio becomes ∼60% for E_f of 14.7 meV. Although the higher-order neutrons do not contaminate the inelastic signal, the intensity normalized by the neutron monitor is reduced by this factor.

III. EXPERIMENTAL RESULTS

A. Dielectric response

Figure 1 shows the temperature dependence of the real (ϵ') and imaginary (ϵ'') parts of the complex dielectric constant at various frequencies; the phase transition temperatures are represented by dotted lines. The cubic-to-tetragonal phase transition occurs at 813 K, and the rhombohedral phase appears at approximately 700 K.[7,8] The tetragonal and rhombohedral phases coexist in a wide temperature range, and the pure rhombohedral phase is observed below 400 K. In the cubic and tetragonal phases, $\epsilon'(T)$ follows the Curie-Weiss law, as shown in Fig. 1(c). The increase in $\epsilon''(T)$ at high temperatures in Fig. 1(b) is associated with the electrical conductivity at high temperatures. Below $T \sim 700$ K, $\epsilon'(T)$ starts to deviate from the Curie-Weiss law, and it shows a broad maximum at $T_m \sim 600$ K. A dielectric dispersion starts to appear below

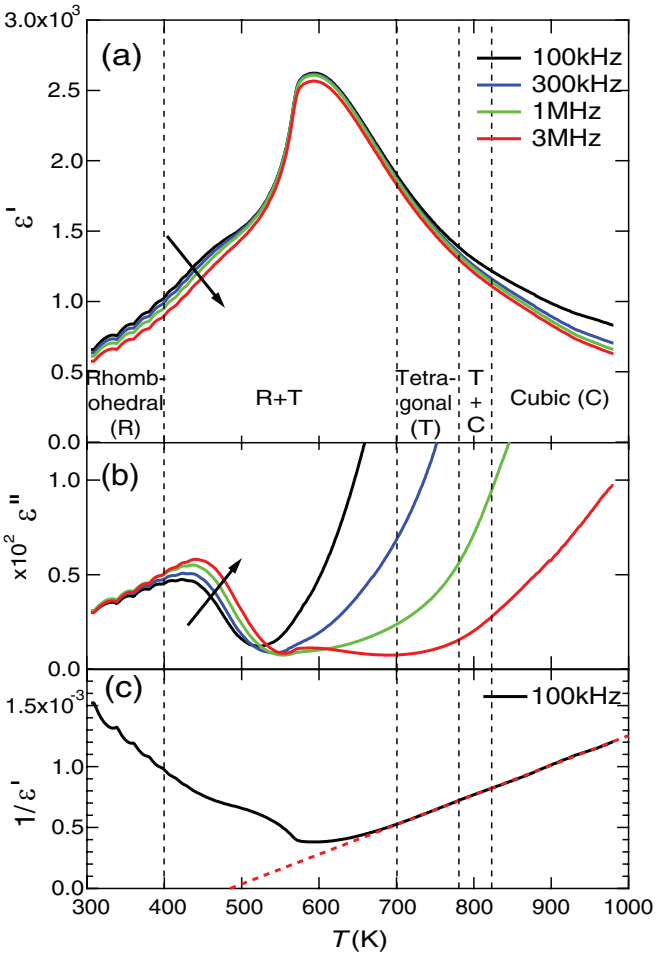

FIG. 1. (Color online) Temperature dependencies of (a) dielectric permittivity ϵ', (b) dielectric loss ϵ'', and (c) the inverse of ϵ' of annealed BNT single crystal measured along the [100] direction during heating. Vertical dotted lines divide the temperature region into areas representing cubic (C), tetragonal (T), and rhombohedral (R) phases and their mixtures. Thick dotted line in (c) represents a fit to the Curie-Weiss behavior for high-temperature data (above 800 K).

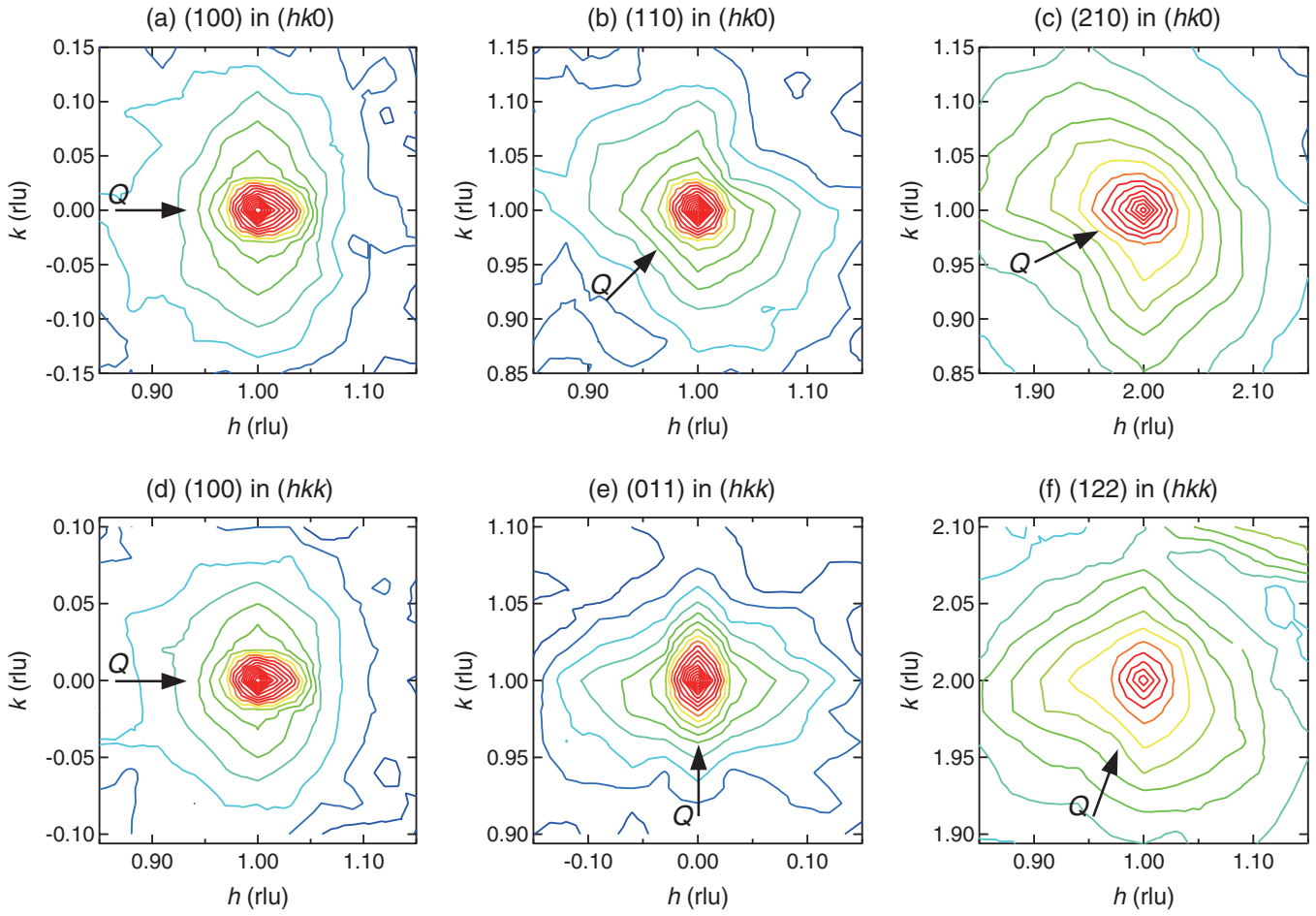

FIG. 2. (Color online) Constant intensity contours of the diffuse scattering near various nuclear Bragg points of BNT measured at $T = 400$ K with E_f of 30.5 meV. Each contour corresponds to a logarithmic change in intensity of 0.2 (base 10). Arrows represent the directions of the wave vector Q for each Bragg reflection. Contours in (a)–(c) were measured in the ($hk0$) scattering plane, whereas those in (d) and (e) were obtained in the (hkk) plane. To compare contours in different zones directly, the contours in the (hkk) zone are plotted in a k range of $-0.106 < k < 0.106$ (rlu) corresponding to the same Q range in Å^{-1} in the ($hk0$) zone.

$T \sim 500$ K on cooling, which is close to the depolarization temperature of 460 $\sim$ 480 K.[9,10] Thus, the broad maximum in $\epsilon'(T)$ and depolarization occur not at the start or end point of structural phase transitions but in the coexisting tetragonal/rhombohedral phase. In addition, T_m exhibits no frequency dependence, which differs markedly from lead-based relaxors.[12]

B. Diffuse scattering

In relaxor ferroelectrics, anisotropic diffuse scattering with a characteristic Q shape, such as a butterfly or ellipsoid pattern, depending on the location in Q space, has been observed near T_m.[13,28] To reveal the origin of the broad maximum in $\epsilon'(T)$, we investigated diffuse scattering around several nuclear Bragg peaks. Figure 2 shows intensity contours of the diffuse scattering on a common logarithmic scale around (110), (100), (210), and (122) measured at $T = 400$ K. Near (100) and (011), ellipsoidal diffuse scattering is observed along the direction transverse to Q, as shown in Figs. 2(a), 2(d), and 2(e). In addition, diffuse scattering with different Q patterns is observed near (110), (210), and (122): a butterfly shape near (110) and asymmetric shapes near (210) and (122), which is consistent with a previous x-ray study.[26] To analyze the anisotropy of the diffuse scattering quantitatively, we plotted the diffuse scattering intensity as a function of the polar angle for the data at $|q| \sim 0.09$ (rlu), where q is the reduced wave vector from a nuclear Bragg point.

The polar plots and their schematic scan trajectory are shown in Fig. 3. Near (100), the diffuse scattering intensity has two peaks at $\theta = -90$ and 90° corresponding to the [010] direction perpendicular to the wave vector Q of (100). Near (110), new peak structures at 0 and 180° also appear, which produce a fourfold peak structure along the ⟨100⟩ direction. In addition, the intensities along the longitudinal direction ($\theta = -135$, 45°) are much weaker than those along the transverse direction ($\theta = -45$, 135°), indicating a transverse nature. Careful inspections of the diffuse scattering near (100) suggest that the longitudinal component exists in the diffuse scattering as shown in Figs. 2(a) and 2(d). However, the longitudinal components near (100) are much weaker than the transverse components, as (110). Near (122), the fourfold peaks at $\theta = -90°, 0°, 90°, 180°$ remain, but the peak at $\theta = 0°$ (90°) is much smaller than that at 180° (−90°), indicating a

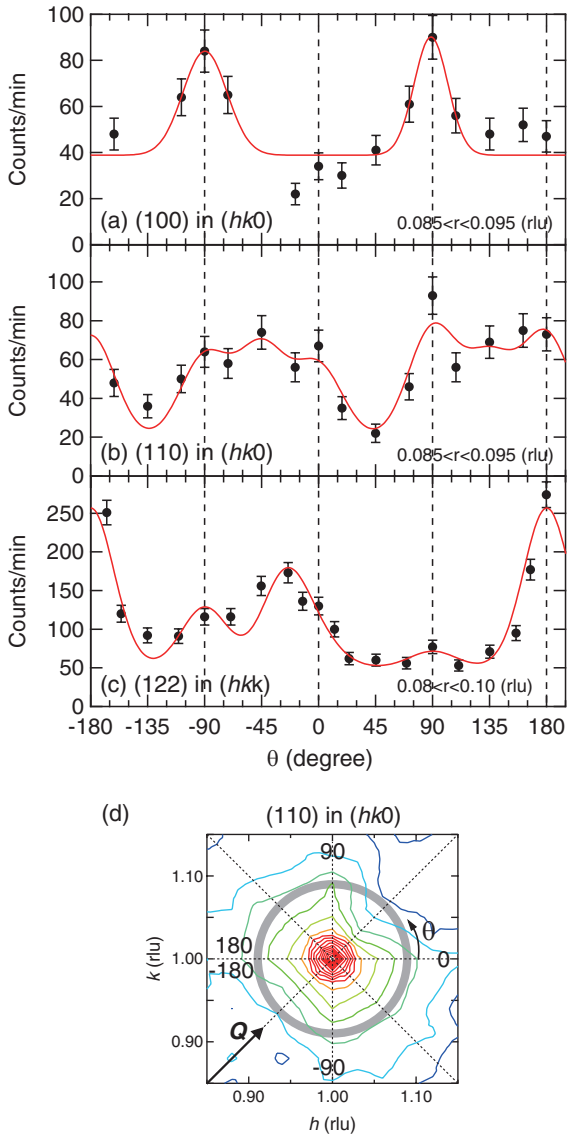

FIG. 3. (Color online) Angle dependence of the diffuse scattering for the radius of $|q| \sim 0.09$ (rlu) around nuclear Bragg peaks (a) (100), (b) (110), and (c) (122) measured at $T = 400$ K. (d) Angle definition and the Q region used in plots (a)–(c) are shown schematically on the intensity contour of diffuse scattering near (110). Data for (a) and (b) were obtained in the (hk0) zone, whereas those for (c) were measured in the (hkk) zone, as shown in Fig. 2.

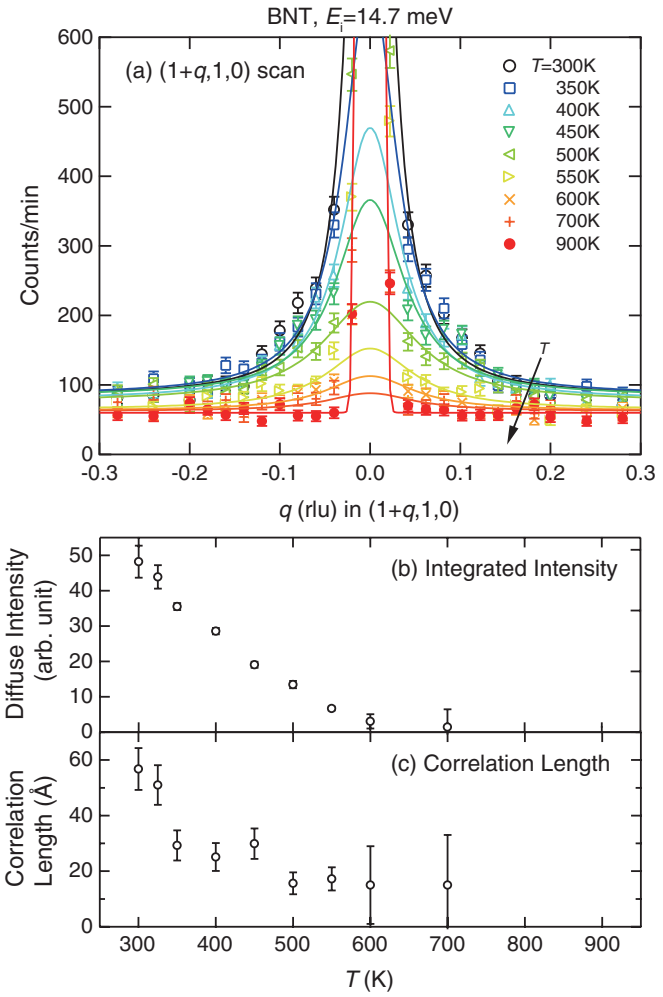

FIG. 4. (Color online) (a) Diffuse scattering measured near (110) along the [100] direction at various temperatures for BNT measured while cooling. Solid lines are fits to the data as described in the text. (b) Temperature dependence of the integrated intensity for the diffuse scattering (open circles). (c) Thermal variation of the correlation length extracted from fits to scans in (a).

greater intensity on the lower-Q side of the Bragg peaks. A similar asymmetry in the diffuse scattering can be seen near (210) [Fig. 2(c)]. The peak at $\theta = -26.5^\circ$ in (122) corresponds to the transverse component. The characteristics of the Q shape of the diffuse scattering can be summarized as follows.

(i) Anisotropy: The intensity ridge extends along the [100] and equivalent directions.

(ii) Transverse nature: The diffuse scattering is strong along the direction perpendicular to Q but weak along the direction parallel to Q, which indicates scattering from ferroelectric fluctuations.

(iii) Asymmetry: The diffuse intensity for the lower-Q side of the Bragg peak is stronger than that for the higher side, especially for Bragg peaks at large Q.

Features (i) and (ii) are similar to those reported for the diffuse scattering in lead-based relaxors with B-site disorder,[13,28] although the direction of anisotropic diffuse scattering is different. On the other hand, similar diffuse scattering with feature (i) and (ii) has been reported in relaxor with A-site disorder $K_{1-x}Li_xTiO_3$.[29] The above features of the diffuse scattering are consistent with previous x-ray studies except for (ii), the transverse feature.[26] The origin of the diffuse scattering and the difference between x-ray and neutron diffraction will be discussed in Sec. IV.

To study the thermal evolution of the anisotropic diffuse scattering in BNT, we performed a Q scan along the [100] direction near (110) at various temperatures between 300 K and 900 K. Figure 4(a) shows the temperature dependence of the peak profile of the diffuse scattering near (110). At $T = 900$ K, there is no diffuse scattering and the profile contains only a narrow resolution-limited (110) peak. A weak diffuse peak appears at 700 K and increases gradually on cooling, which is consistent with the pioneering work of Vakhrushev *et al.*[23]

The profiles were fitted to the sum of a broad Lorentzian and a narrow Gaussian function of q, corresponding to the diffuse scattering and the (110) Bragg peak, respectively. The obtained integrated intensities for the diffuse scattering are plotted as a function of temperature in Fig. 4(b) and Fig. 10(a). The onset temperature of the diffuse scattering at the Γ point of 700 K coincides with the deviation from the Curie-Weiss behavior in the dielectric constant shown in Fig. 1(c). The correlation length ξ is determined from the inverse of the half-width at half-maximum $\kappa = 1/\xi$, as shown in Fig. 4(c). Above 500 K, ξ is constant at ∼10 Å. Then ξ gradually increases below 450 K and reaches 57 ± 8 Å at 300 K. Thus, both the intensity and correlation length of the diffuse scattering show no enhancement near T_m, which differs substantially from the diffuse scattering in lead-based relaxors.[30,31]

Two of the authors recently succeeded in growing high-quality BNT single crystals showing lower leakage current and better polarization switching by developing new crystal growth methods under high oxygen pressure.[10,27] They succeeded in increasing remanent polarization, which was attributed to a reduction in the clamped domain walls at oxygen vacancies. As for the growth condition dependence of the broad maximum temperature of the dielectric constant and the depolarization temperature, we confirmed that these temperatures do not depend on the atmosphere of crystal growth. To study the correlation between the diffuse scattering and atom vacancies, we performed the same Q scan as in Fig. 4(a) for the high-quality single crystals grown under various oxygen pressures (P_{O_2}). The peak profiles of the Q scan for BNT single crystals grown under air and $P_{O_2} = 0.2$ and 10 atm are shown in Fig. 5. In order to compare diffuse scattering grown under different conditions, profiles are plotted on the same intensity scale after normalizing the data by crystal volume and counting time. The crystal grown under high P_{O_2} clearly shows less diffuse scattering than that grown under low P_{O_2}. We repeated the same procedure for several crystals and obtained a similar trend: larger diffuse scattering for crystals grown with less oxygen pressure. This result indicates a close correlation between crystal defects and diffuse scattering. However, the diffuse scattering loses almost all of its intensity at $T = 700$ K,

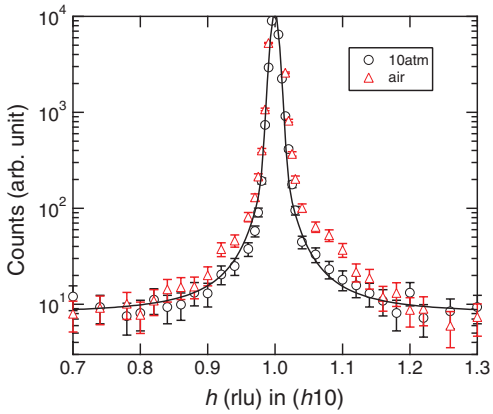

FIG. 5. (Color online) Diffuse scattering measured near (110) along the [100] direction at $T = 300$ K for BNT crystals grown under air and under oxygen pressures of 10 atm. The intensities are normalized by crystal volume and counting time.

as shown in Fig. 4, which is unexpected for defect-origin Huang scattering. The other possible explanation for the above observation will be discussed in Sec. IV.

C. Lattice dynamics

By analogy with the diffuse scattering in lead-based relaxors, the observed temperature-dependent diffuse scattering near the Γ point suggests the appearance of small polar clusters at temperatures much higher than that of the pure rhombohedral phase (below 400 K). However, the diffuse scattering does not show any anomaly near T_m, as described in the previous section. To study lattice instabilities near T_m and the depolarization temperature, we investigated phonon dispersions of transverse modes near (220). Figures 6(a)–6(c) show constant-Q scans at $T = 400$ and 670 K. At $q = 0$, there is no clear phonon peak in the spectra at 670 K, whereas a small shoulder appears at $\hbar\omega = 11.6$ meV at 400 K, as indicated by the thick arrow. The TO mode near the Γ point is not visible because the TO mode for $q < 0.10$ is heavily overdamped at 670 K. At $q = 0.15$, well-defined transverse acoustic (TA) and TO modes are observed at both 400 and 670 K. The TO mode at 670 K clearly appears at a lower energy than that at 400 K, which indicates softening of the TO mode at 670 K. A similar trend in the soft TO mode is also observed at $q = 0.20$. On the other hand, the TA mode at $q = 0.20$ becomes soft at 400 K, which leads to a flat TA dispersion near the zone boundary at 400 K. When the dispersion drops dramatically at some q values, a constant-energy scan is better than a constant-Q scan to find a phonon peak in (Q,ω) space. Figures 6(d)–6(f)

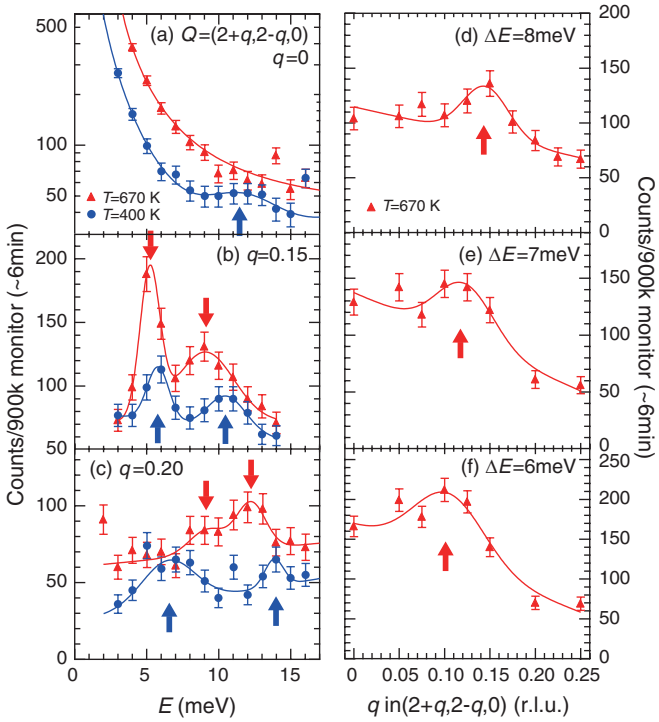

FIG. 6. (Color online) [(a)–(c)] Constant-Q scans at $(2+q,2-q,0)$ and [(d)–(f)] constant-energy scans at various energies measured at $T = 670$ and 400 K with fixed $E_f = 14.7$ meV. Intensity for $q = 0$ is plotted on a logarithmic scale to show the small peak clearly. Arrows indicate peak positions summarized in Fig. 7 and Fig. 8(b).

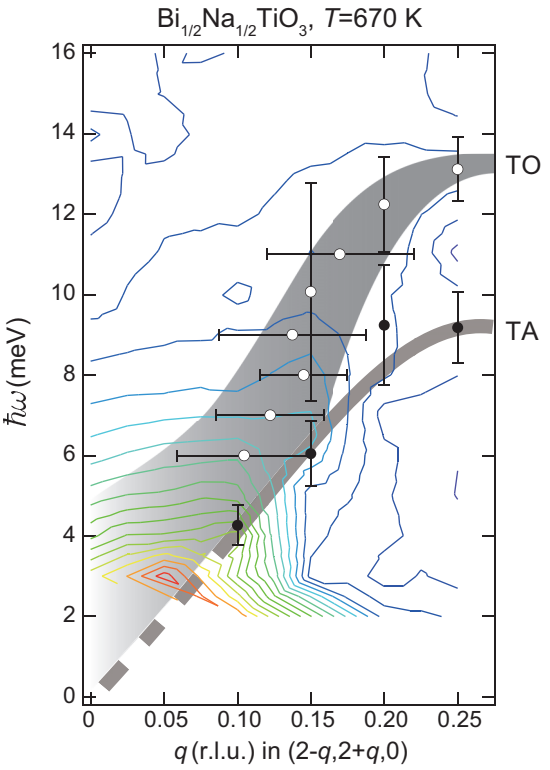

FIG. 7. (Color online) Contour map of the phonon-scattering intensity near (220) measured at $T = 670$ K with fixed $E_f = 14.7$ meV. Each contour corresponds to a logarithmic change in intensity of 0.1 (base 10). Open and closed circles show the peak positions of the TA and TO modes, respectively, obtained from Fig. 6. The error bars represent the half-width at half-maximum. The shaded area and the thick line schematically represent the TO and TA dispersions, respectively.

show constant-energy scans at $\hbar\omega = 6$, 7, and 8 meV for this purpose. A broad peak structure is observed at $q = 0.10$ ($\hbar\omega = 6$ meV), 0.12 (7 meV), and 0.15 rlu (8 meV), indicating a sharp drop in the TO branch near $q \sim 0.12$.

Figure 7 summarizes the TA and TO dispersions at $T = 670$ K overplotted on the constant intensity contours of the phonon scattering near (220). The TO mode becomes soft and drops sharply at $q \sim 0.12$, which is very similar to those reported in the classical relaxor PZN-8%$PbTiO_3$ (PT)[14] and PMN,[15] the "waterfall" anomaly. Although no clear phonon peak is observed near the Γ point for $q \leqslant 0.10$, the intensity of the overdamped soft TO mode is substantial, as is clear from the contours. Therefore, we schematically show the dispersion of the overdamped soft mode by a shaded area.

As shown in Fig. 6(a), the waterfall feature disappears and the soft mode recovers at $T = 400$ K, which coincides roughly with the depolarization temperature. To study the temperature dependence of the soft TO branch, we performed a constant-energy scan at $\hbar\omega = 8$ meV at various temperatures [Fig. 8(a)]. The peak structure at which the waterfall intersects $\hbar\omega = 8$ meV shifts from $q = 0.15$ to 0.10 on cooling from $T = 670$ K to 500 K. Below $T = 400$ K, the peak structure disappears in the constant-energy scan at $\hbar\omega = 8$ meV. Together with the results of constant-Q scans at 400 K, this result indicates that the soft mode near the Γ point becomes

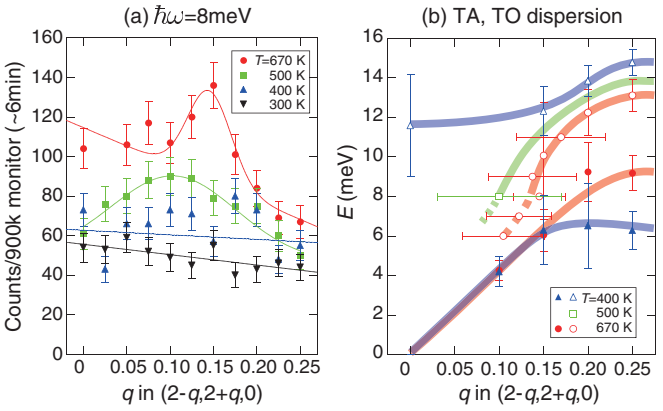

FIG. 8. (Color online) (a) Constant-energy scans near (220) along the [$\bar{1}$10] direction at $\hbar\omega = 8$ meV measured at various temperatures with fixed $E_f = 14.7$ meV. Solid lines show fits to the Gaussian function on a sloped background. (b) TA and TO dispersions along the [$\bar{1}$10] direction intensity near (220) at $T = 670$ K, 500 K, and 400 K. The thick lines are guides to the eye for TO and TA dispersions.

harder than 8 meV at 400 K. Figure 8(b) summarizes the thermal variation in the TA and TO branches. In the coexisting tetragonal/rhombohedral phase between 400 and 700 K, the soft mode becomes hard as the temperature decreases but it is still overdamped near the Γ point down to 500 K. It then eventually recovers at temperatures between 400 and 500 K, which is close to the depolarization temperature of 460 ∼ 480 K.

The overdamped soft mode near the Γ point in the coexisting tetragonal and rhombohedral phases indicates the dynamic nature of polar clusters in the coexisting phase. To study the energy dependence of the anisotropic diffuse scattering at finite q, we compare constant-Q scans at (2.15,1.85,0) (where the anisotropic diffuse scattering is weak) and (3,−0.21,0) (where the anisotropic diffuse scattering is strong). Figure 9 shows the energy spectrum at these Q measured in the cubic phase ($T = 820$ K), coexisting tetragonal/rhombohedral phase (600 K), and rhombohedral phase (400 K). At $T = 820$ K, the TA mode at (3,−0.21,0) is heavily overdamped, whereas an underdamped TA mode is observed at 4.5 meV for (2.15,1.85,0). A mismatch between the instrumental resolution and the dispersion surface can cause significant spectral broadening, which is known as the "defocused" condition. However, this is not the case here because these Q points are in the "focused" condition for the current experimental setup (right-handed triple-axis spectrometer). Thus, the TA mode is not isotropic: It is soft and overdamped for the [0$\bar{1}$0] direction, which is the same direction as the anisotropic diffuse scattering. Since the diffuse scattering is reduced for crystals grown under high oxygen pressure, the damping of acoustic mode may be weakened for such high-quality crystals, which will require further study. On cooling, the appearance of a small shoulder at $\hbar\omega \sim 4$ meV ($T = 600$ K) and 5 meV ($T = 400$ K) indicates the recovery of the TA mode at (3,−0.21,0). However, the recovered TA mode at (3,−0.21,0) is still softer and broader than that at (2.15,1.85,0). In addition, substantial quasielastic scattering remains at $T = 400$ and 600 K for (3, −0.21,0) that is absent at (2.15,1.85,0). These results indicate that BNT has phase instabilities with the same origin as that of the

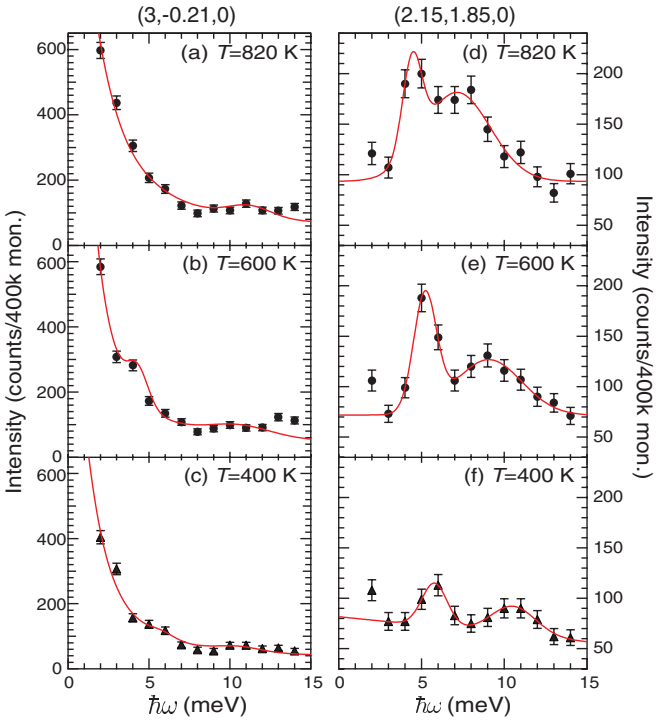

FIG. 9. (Color online) Constant-Q scans at [(a)–(c)] (3,−0.21,0) and [(d)–(f)] (2.15,1.85,0) measured at various temperatures with fixed $E_f = 30.5$ meV. The solid lines are fits to a sum of Lorentzian and Gaussian functions for (a)–(c) and to a sum of two Gaussian functions for (d)–(f). A clear TO mode was not observed at (3,−0.21,0), indicating a small structural factor.

diffuse scattering: a competition between the rhombohedral and tetragonal phases.

IV. DISCUSSIONS

A. Diffuse scattering

We observed anisotropic diffuse scattering extending along the ⟨100⟩ and equivalent directions near the Γ point for $T \leqslant 700$ K. Here we discuss the correlation between the diffuse scattering near the Γ point and the dielectric and ferroelectric properties of BNT. Figure 10(a) shows the thermal variations in the dielectric constant measured at 1 MHz and the integrated intensity of diffuse scattering near the Γ point. The intensities of the superlattice peaks at the M point $(\frac{1}{2},\frac{3}{2},0)$ and the R point $(\frac{3}{2},\frac{1}{2},\frac{1}{2})$ are overplotted as a function of temperature. Although the cubic-to-tetragonal phase transition has been reported at $T = 813$ K, the M point peak was observed up to 900 K. The component above 813 K is presumably the quasielastic scattering reported previously, which persists up to ∼900 K.[8] The diffuse scattering intensity gradually grows on cooling below 700 K and shows no rapid increase at $T_m \sim 600$ K, at which the dielectric constant has a broad maximum. This differs markedly from PMN; the diffuse intensity grows as $\epsilon'(T)$ near T_m,[30,31] as shown in Fig. 10(b). In addition, T_m exhibits no frequency dependence in BNT. The disagreement between the thermal variation of the dielectric constant and the diffuse scattering and the lack of dielectric

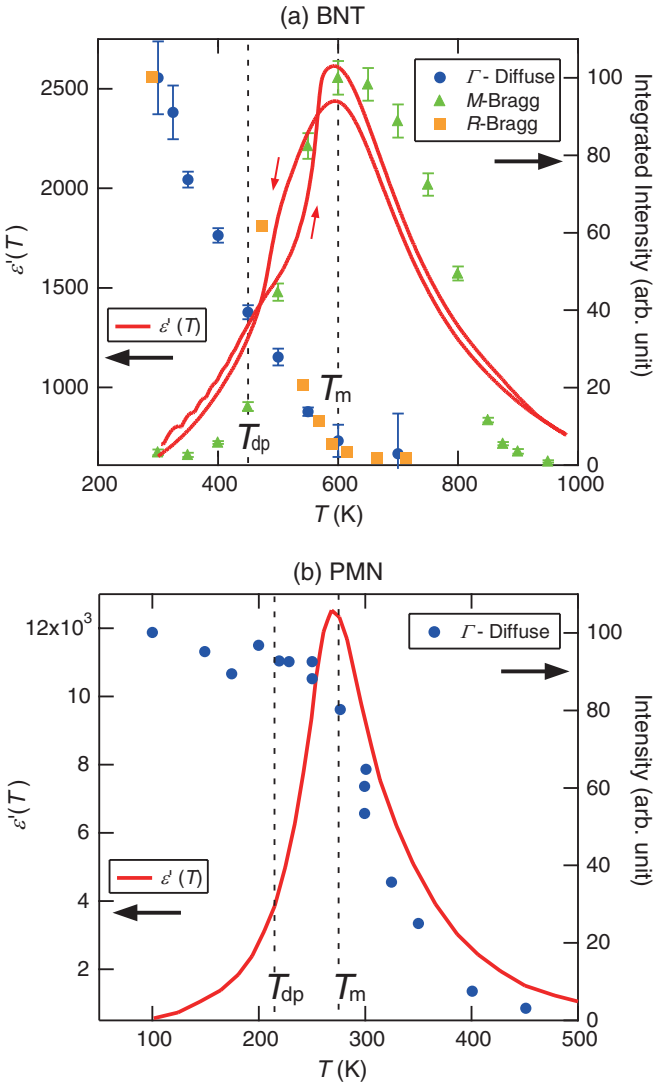

FIG. 10. (Color online) Temperature dependence of the dielectric constant measured at 1 MHz and the intensity of the diffuse scattering near the Γ point (Γ diffuse) for (a) BNT and (b) PMN. The dielectric constant data for BNT are the same as in Fig. 1 and those for PMN are from Ref. 26. The intensities of diffuse scattering for BNT are q integrated as in Fig. 4, whereas those for PMN are the values at $(1-q,1+q,0)$ with $q = 0.05$ measured by Hiraka *et al.* (Ref. 23) using cold neutrons. For (a) BNT, the intensities of the superlattice peak at the M point $(\frac{1}{2},\frac{3}{2},0)$ (M-Bragg) (current study) and the R point $(\frac{3}{2},\frac{1}{2},\frac{1}{2})$ (R-Bragg) (Ref. 8) are overplotted. The intensities of the diffuse scattering near the Γ point and those of the Bragg peak at the M point are normalized to 100 by their respective maximum values. The vertical dotted lines show the temperature at which the dielectric constant has the maximum (T_m) and at which depolarization occurs (T_{dp}).

dispersion near T_m indicate different origins of the broad maximum in the dielectric constant in BNT and lead-based relaxors.

Note that the $\epsilon'(T)$ resembles the intensity of the superlattice peak at the M point. In general, susceptibility becomes large toward phase transition and suppressed as temperature decreases below the transition temperature. In BNT, the

tetragonal phase appears at 813 K,[7] Therefore, the increase in the dielectric constant on cooling below 813K could not be explained by the development of *stable* tetragonal phase. Instead, the rhombohedral and tetragonal phases coexist in a wide temperature range between 400 and 700 K.[7,8] In addition, a quasielastic scattering has been observed at the R point below 1020 K,[22] which indicates competition between the tetragonal and rhombohedral phases from much high temperatures above 700 K. Furthermore, a large hysteresis in the dielectric constant [Fig. 10(a)] and the intensities of the superlattice peaks at the M and R points[8] have been observed at the transition from the tetragonal to the rhombohedral phase. Although no discontinuity in the dielectric constant has been observed, these results indicate a first-order transition from the tetragonal to the rhombohedral phase. It is possible that random occupation of the A site in the ABO_3 structure by Na^+ and Bi^{3+} cations causes diffusive phase transitions. It is known that susceptibility does not diverge significantly for a first-order transition because a transition occurs at higher temperatures than the divergence temperature. Because the broad maximum in $\epsilon'(T)$ for BNT appears at roughly the onset temperature of the superlattice peak at the R point, as shown in Fig. 10, the broad maximum in $\epsilon'(T)$ could be associated with the diffusive first-order transition from the tetragonal to the rhombohedral phase. The resemblance of the $\epsilon'(T)$ and the intensity of the superlattice peak at the M point then is presumably due to the increase of a *metastable* tetragonal phase.

We observed a qualitative difference in the Q pattern of the diffuse scattering between x-ray and neutron diffraction. Near (100), the x-ray study showed diffuse scattering along the [100] direction, which is longitudinal to Q,[26] whereas the current neutron study finds a much stronger diffuse intensity along the [010] direction, which is transverse to Q. The possible explanation for this discrepancy is the difference in scattering power between x-rays and neutrons. The scattering length for x-rays is proportional to the number of electrons Z, whereas that for neutrons, with a scattering length b, has no regularity with respect to Z. The number of electrons Z for Bi^{3+} is much larger than those for the other ions. In addition, larger atomic displacement of Bi^{3+} than the other ions has been reported from neutron powder diffraction study.[7] Thus, the main contribution to the diffuse scattering obtained by x-rays is the atomic displacement of Bi^{3+}, whereas the diffuse scattering in the neutron study includes an atomic shift of all atoms with the same order. In addition, the neutron scattering length for Ti ion is negative, which produces a large structure factor for the antiparallel shift between Bi/Na and Ti and a small one for the parallel shift. As described in the Introduction, such antiparallel cation shifts of Bi/Na and Ti are realized in the tetragonal phase. Moreover, the antiparallel cation shifts are along the fourfold axis of the tetragonal phase, which is consistent with the diffuse intensity rods along the ⟨100⟩ and equivalent directions.

In addition to the difference in scattering power between x-rays and neutrons, the difference in energy resolution could also be used to explain the discrepancy between the x-ray and neutron measurements. The typical energy resolution for the current neutron scattering study is ∼1 meV at elastic conditions, whereas x-ray diffraction using high-energy x-rays with $\lambda = 0.3738$ Å ($E = 33.2$ keV) includes elastic and all phonon scattering because of its coarse energy resolution, on the order of eV. As shown in Fig. 9(b), the overdamped soft acoustic phonon appears only along the [010] direction, which is transverse to Q. The strong scattering at low energies from the overdamped soft TA mode can contribute greatly to the diffuse scattering intensity when the signal is obtained near the elastic channel within ±1 meV.

We confirmed the asymmetric diffuse scattering reported in the x-ray study.[26] The larger intensity for the lower-Q side of the Bragg peaks indicates that the small regions responsible for the diffuse scattering have larger unit cells than the surrounding matrix. From a Monte Carlo simulation of the x-ray data, Kreisel *et al.* suggested that large Bi-Bi bonding (∼2%) and small Na-Na bonding in planar defects could be the origin of the asymmetric diffuse scattering. They reproduced the observed diffuse scattering pattern by assuming the above displacements with a thickness of two unit cells. However, our neutron study shows a correlation length of 60 Å at $T = 300$ K, which corresponds to ∼15 unit cells. It cannot be expected that such large bonding coherently exists only for Bi-Bi bonds in 15 unit cells. Instead, the fact that the tetragonal lattice parameter c_T is larger than the rhombohedral lattice parameter a_R naturally explains the stronger ⟨100⟩-diffuse scattering on the lower-Q side of the Bragg peaks. Thus, atomic shifts bridging the rhombohedral and tetragonal phases from the ideal position of the rhombohedral phase can explain both the anisotropy and asymmetry of the observed diffuse scattering.

Another important finding in the current study of diffuse scattering is that the diffuse intensity is reduced in high-quality samples grown under high oxygen pressure. This does not mean that the diffuse scattering originates in defects (Huang scattering) because the disappearance of the diffuse scattering at 700 K cannot be explained by the Debye-Waller factor. Although significant softening of the elastic constant on heating toward 600 K has been reported,[32] this should produce the opposite change: larger Huang scattering at high temperatures toward ∼600 K. Instead, the smaller diffuse scattering for the sample with fewer Bi/O vacancies can be associated with a long time trap of soft phonons at these vacancies,[33] as discussed for hydrogen-reduced $SrTiO_3$.[34] Together with the transverse nature and asymmetric shape of the diffuse scattering, we speculate that the origin of the diffuse scattering could be associated with correlated atomic shifts in polar metastable clusters with low crystal symmetry which are trapped near oxygen deficiencies.

B. Lattice dynamics

Vakhrushev *et al.* investigated the lattice dynamics at high-symmetry points at zone boundaries in BNT and found strong quasielastic scattering at the M point below 900 K and at the R point below 1020 K.[8,22] Together with our observation of the damped soft mode at the Γ point, this suggests that quasielastic scatterings at the Γ, M, and R points coexist for $400 \leqslant T \leqslant 700$ K in BNT. The coexistence of the soft modes at the Γ and R points can be understood from the rhombohedral structure $R3c$ in BNT because it involves an antiphase tilt of the TiO_6 octahedra about the threefold pseudocubic axes and parallel cation shifts along the polar axes, which

correspond to two irreducible representations, R_{25} and Γ_{15}, respectively.[22] This simplifies the lattice dynamics in BNT to the competition between the rhombohedral and tetragonal phases.

Although hardening of the soft mode near the Γ point is suggested by the peak shift toward low q in the constant-energy profile (Fig. 8), the soft mode is heavily overdamped in the coexisting tetragonal/rhombohedral phase. The damped phonon spectra equals to quasielastic scattering for large damping, as shown in Fig. 6(a). Quasielastic scattering means that the correlation function is rapidly attenuated within a characteristic relaxation time, which is inversely proportional to the peak width. The observed quasielastic scattering with a linewidth on the order of meV indicates a relaxation time on the order of picoseconds. Thus, the atoms responsible for quasielastic scattering are expected to hop among metastable states on a picosecond time scale, which could lead to depolarization. As the temperature is reduced, the ferroelectric order is supposed to be stabilized when atoms cannot overcome the potential barriers separating the quasistable states. We observed the recovery of the soft mode and the disappearance of the waterfall feature at 400 K, which indicates such a stabilization of the ferroelectric state. Furthermore, the waterfall feature disappears at roughly the depolarization temperature. These results indicate that the depolarization originates in the dynamic nature of the rhombohedral phase in the coexisting tetragonal/rhombohedral phase. We should mention that a mesoscopic or macroscopic rhombohedral region, which is believed to be well stabilized, is established in some parts of the crystal below 600 K. The depolarization between 400 and 600 K indicates that polarizations in mesoscopic/macroscopic domains are affected by fluctuations of polarizations in small clusters. When the size distribution of domains is sufficiently discrete, fluctuations in different hierarchical domains can be treated as adiabatic changes, that is, scale separation. However, when the size distribution of domains is continuous or not sufficiently discrete, fluctuations in small domains could couple to those in mesoscopic/macroscopic domains. This possibility requires further study of the dynamics in mesoscopic domains bridging microscopic and macroscopic domains.

It is worth noting that the remanent polarization in PMN develops rapidly at ∼213 K,[35] below which the waterfall feature disappears.[36] This similarity suggests a common depolarization mechanism in BNT and PMN. A recent neutron scattering study of PMN by Swainson *et al.* reported that overdamped soft modes exist not only at the Γ point but also at the M and R points.[37] All of the soft modes in PMN have a minimum frequency at 400 K and quasielastic scatterings exist down to 213 K, indicating the existence of metastable states, as in BNT. Thus, competition between lattice instabilities with different crystal symmetries may explain the lack of remanent polarization between 213 and 400 K in PMN.

We found that the waterfall feature disappears when the tetragonal phase disappears. The damping of phonon modes simply indicates energy dissipation from phonon modes to the other degree of freedom. One possible origin of phonon damping is coupling to other phonon modes through the anharmonic potential in a homogeneous lattice. However, this scenario cannot be used for an inhomogeneous lattice, which is realized in the coexisting tetragonal/rhombohedral phase of BNT. On the other hand, Yamada and Takakura explained the watefall feature in PMN by treating the displacement of Pb^{2+} ions as a pseudospin and considering a mode coupling between random motion of pseudospins and the soft mode.[38] Recently, Matsuura *et al.* also have succeeded in describing an overdamped phonon spectrum in PMN-30%PT by use of the pseusospin-phonon coupled model.[39] For BNT, quasielastic scattering at the Γ, R, and M points coexist between 400 and 700 K, indicating metastable tetragonal and rhombohedral phases in this temperature region. In addition, large displacements of A-site cations Bi^{3+} and Na^{+} have been reported from a power neutron diffraction study.[7] Random hopping of Bi^{3+} and Na^{+} ions among these metastable states in the coexisting tetragonal/rhombohedral phase then could possibly couple with soft modes in BNT, which could produce overdamped phonon spectra.

In addition to the soft TO mode near the Γ point, we observed the overdamped soft TA mode along the same direction as the strong anisotropic diffuse scattering. A similar overdamped soft TA mode at the same Q as the strong anisotropic diffuse scattering has been observed in PMN[40,41] and has been associated with high piezoelectricity in PMN. In addition, a recent neutron powder diffraction study suggested that the true lattice symmetry of the rhombohedral phase of BNT is monoclinic with space group Cc.[42] If the symmetry of the lowest temperature phase of BNT is monoclinic, the phase transition sequence of BNT is the same as those in the MPB region of PMN-PT: cubic to tetragonal and tetragonal to monoclinic on cooling. Despite the resemblance to the MPB, the piezoelectric coefficients of BNT are relatively low.[1] Thus, the monoclinic structure and its structural instability seem to have no correlation with the piezoelectricity in BNT. However, there is an important difference between BNT and lead-based relaxors: the tetragonal phase is ferrielectric with small polarization for BNT, whereas it is ferroelectric for the lead-based relaxors. If the polarization in the tetragonal phase is small, the polarization in the monoclinic phase that bridges the rhombohedral and tetragonal structure could become smaller than that in the rhombohedral phase, which may reduce the magnitude of the polarization during rotation. Further measurements are clearly required to provide evidence of possible polarization rotation in BNT.

V. SUMMARY

We studied the diffuse scattering and lattice dynamics near the Γ point in $(Bi_{1/2}Na_{1/2})TiO_3$ using neutron scattering to elucidate the complex depolarization process and structural phase sequence. We observed diffuse scattering near the Γ point with an anisotropic Q shape extending along the ⟨100⟩ directions transverse to the scattering vector Q below 700 K, which is associated with a deformed rhombohedral structure bridging the rhombohedral and tetragonal phases. From the temperature dependencies of the dielectric constant, diffuse scattering near the Γ point, and superlattice peaks at the M and R points, we propose that the broad maximum in the dielectric constant originates in a diffusive first-order transition between the competing tetragonal and rhombohedral phases. We found the heavily overdamped soft transverse optical mode near the

Γ point and the overdamped transverse acoustic mode along the ⟨100⟩ directions in the coexisting tetragonal/rhombohedral phase, which is quite similar to those reported in lead-based relaxors. The recovery of the underdamped soft mode coincides with the increase in the remanent polarization, which can be explained by the stabilization of the ferroelectric rhombohedral phase due to the disappearance of the competing tetragonal state.

ACKNOWLEDGMENTS

We are grateful to T. Sato and Y. Yamaguchi for their stimulating discussions. The INS experiments at PONTA and HQR were performed under a joint research program of ISSP the University of Tokyo. M.M., K.O., Y.N., and K.H. were supported by a Grant-in-Aid for Scientific Research on Priority Areas "Novel States of Matter Induced by Frustration" (19052002).

[1] G. A. Smolenskii, V. A. Isupov, A. I. Agranovskaya, and N. N. Krainik, Fiz. Tverd. Tela (Leningrad) **2**, 2982 (1960) [Sov. Phys. Solid State **2**, 2651 (1961)].

[2] V. A. Isupov, Ferroelectrics **315**, 123 (2005).

[3] T. Takenaka and K. Sakata, Ferroelectrics **95**, 153 (1989).

[4] T. Takenaka, K. Sakata, and K. Toda, Ferroelectrics **106**, 375 (1990).

[5] T. Takenaka, K. Maruyama, and K. Sakata, Jpn. J. Appl. Phys. **30**, 2236 (1991).

[6] K. Sakata and Y. Masuda, Ferroelectrics **7**, 347 (1974).

[7] G. O. Jones and P. A. Thomas, Acta Crystallogr. Sect. B **58**, 168 (2002).

[8] S. B. Vakhrushev, B. E. Kvyatkovskii, N. M. Okuneva, E. L. Plachenova, and P. P. Syrnikov, Pis'ma Zh. Eksp. Teor. Fiz. **35**, 111 (1982) [JETP Lett. **35**, 134 (1982)].

[9] Y. Hiruma, H. Nagata, and T. Takenaka, J. Appl. Phys. **105**, 084112 (2009).

[10] M. Suzuki, A. Morishita, Y. Kitanaka, Y. Noguchi, and M. Miyayama, Jpn. J. Appl. Phys. **49**, 09MD09 (2010).

[11] G. Burns and F. H. Dacol, Solid State Commun. **48**, 853 (1983).

[12] D. Viehland, S. J. Jang, L. E. Cross, and M. Wuttig, J. Appl. Phys. **68**, 2916 (1990).

[13] S. B. Vakhrushev, A. A. Naberezhnov, N. M. Okuneva, and B. N. Savenko, Fiz. Tverd. Tela (St. Petersburg) **37**, 3621 (1995) [Sov. Phys. Solid State **37**, 1993 (1995)].

[14] P. M. Gehring, S. E. Park, and G. Shirane, Phys. Rev. Lett. **84**, 5216 (2000).

[15] P. M. Gehring, S. Wakimoto, Z. G. Ye, and G. Shirane, Phys. Rev. Lett. **87**, 277601 (2001).

[16] P. M. Gehring, S. E. Park, and G. Shirane, Phys. Rev. B **63**, 224109 (2001).

[17] S. Vakhrushev, A. Ivanov, and J. Kulda, Phys. Chem. Chem. Phys. **7**, 2340 (2005).

[18] P. Ganesh, E. Cockayne, M. Ahart, R. E. Cohen, B. Burton, R. J. Hemley, Y. Ren, W. Yang, and Z.-G. Ye, Phys. Rev. B **81**, 144102 (2010).

[19] A. Cervellino, S. N. Gvasaliya, O. Zaharko, B. Roessli, G. M. Rotaru, R. A. Cowley, S. G. Lushnikov, T. A. Shaplygina, and M. T. Fernandez-DiazJ. Appl. Crystallogr. **44**, 603 (2011).

[20] A. Bosak, D. Chernyshov, S. Vakhrushev, and M. Krisch, Acta Crystallogr. Sect. A **68**, 117 (2012).

[21] M. Pasciak, T. R. Welberry, J. Kulda, M. Kempa, and J. Hlinka, Phys. Rev. B **85**, 224109 (2012).

[22] S. B. Vakhrushev, B. E. Kvyatkovskii, N. M. Okuneva, E. L. Plachenova, and P. P. Syrnikov, Fiz. Tverd. Tela (Leningrad) **25**, 2529 (1983) [Sov. Phys. Solid State **25**, 1456 (1983)].

[23] S. B. Vakhrushev, B. E. Kvyatkovskii, R. S. Malysheva, N. M. Okuneva, and P. P. Syrnikov, Fiz. Tverd. Tela (Leningrad) **27**, 737 (1985) [Sov. Phys. Solid State **27**, 455 (1985)].

[24] S. B. Vakhrushev, B. E. Kvyatkovskii, R. S. Malysheva, N. M. Okuneva, E. L. Plachenova, and P. P. Syrnikov, Kristallografiya **34**, 154 (1989) [Sov. Phys. Crystallogr. **34**, 89 (1989)].

[25] A. M. Balagurov, E. Y. Koroleva, A. A. Naberezhnov, V. P. Sakhnenko, B. N. Savenko, N. V. Ter-Oganessian, and S. B. Vakhrushev, Phase Transitions **79**, 163 (2006).

[26] J. Kreisel, P. Bouvier, B. Dkhil, P. A. Thomas, A. M. Glazer, T. R. Welberry, B. Chaabane, and M. Mezouar, Phys. Rev. B **68**, 014113 (2003).

[27] Y. Kitanaka, H. Onozuka, Y. Noguchi, and M. Miyayama, Ferroelectrics **414**, 24 (2011).

[28] G. Xu, G. Shirane, J. R. D. Copley, and P. M. Gehring, Phys. Rev. B **69**, 064112 (2004).

[29] S. Wakimoto, G. A. Samara, R. K. Grubbs, E. L. Venturini, L. A. Boatner, G. Xu, G. Shirane, and S.-H. Lee, Phys. Rev. B **74**, 054101 (2006).

[30] V. Bovtun, S. Kamba, A. Pashkin, M. Savinov, P. Samoukhina, J. Petzelt, P. Bykov, and M. D. Glinchuk, Ferroelectrics **298**, 23 (2004).

[31] H. Hiraka, S.-H. Lee, P. M. Gehring, G. Xu, and G. Shirane, Phys. Rev. B **70**, 184105 (2004).

[32] J. Suchanicz, J. Mater. Sci. **37**, 489 (2002).

[33] B. I. Halperin and C. M. Varma, Phys. Rev. B **14**, 4030 (1976).

[34] J. B. Hastings, S. M. Shapiro, and B. C. Frazer, Phys. Rev. Lett. **40**, 237 (1978).

[35] D. Fu, H. Taniguchi, M. Itoh, S. Y. Koshihara, N. Yamamoto, and S. Mori, Phys. Rev. Lett. **103**, 207601 (2009).

[36] S. Wakimoto, C. Stock, R. J. Birgeneau, Z. G. Ye, W. Chen, W. J. L. Buyers, P. M. Gehring, and G. Shirane, Phys. Rev. B **65**, 172105 (2002).

[37] I. P. Swainson, C. Stock, P. M. Gehring, G. Xu, K. Hirota, Y. Qiu, H. Luo, X. Zhao, J.-F. Li, and D. Viehland, Phys. Rev. B **79**, 224301 (2009).

[38] Y. Yamada and T. Takakura, arXiv:cond-mat/0209573 (unpublished) (2002).

[39] M. Matsuura, H. Hiraka, K. Yamada, and K. Hirota, J. Phys. Soc. Jpn. **80**, 104601 (2011).

[40] C. Stock, H. Luo, D. Viehland, J. F. Li, I. P. Swainson, R. J. Birgeneau, and G. Shirane, J. Phys. Soc. Jpn. **74**, 3002 (2005).

[41] G. Xu, J. Wen, C. Stock, and P. M. Gehring, Nat. Mater. **7**, 562 (2008).

[42] E. Aksel, J. S. Forrester, J. L. Jones, P. A. Thomas, K. Page, and M. R. Suchomel, Appl. Phys. Lett. **98**, 152901 (2011).